Microcracking of composites reinforced by stitched multiaxials subjected to cyclical hygrothermal loadings

Pierre-Jacques Liotier, Alain Vautrin, Jean-Marc Béraud

Microcracking of composites reinforced by stitched multiaxials subjected to cyclical hygrothermal loadings

Pierre-Jacques Liotier [a,*], Alain Vautrin [a], Jean-Marc Beraud [b]

[a] LTDS, École Nationale Supérieure des Mines de Saint-Étienne 158, cours Fauriel, F-42023 Saint-Étienne Cedex 2, France
[b] HEXCEL Reinforcements, ZI les Nappes 38630 Les Avenières, France

Microcracking of polymer matrix composites reinforced by multiaxial multi-ply stitched carbon preforms submitted to cyclical purely hygrothermal loading is analyzed. The laminates are manufactured by liquid resin infusion (LRI). The stitching induces deviations in fibre layout and creates openings which become resin-rich regions after the resin infusion. The interaction between resin-rich regions and microcracks induced by the hygrothermal cycles was investigated by 2D metallographic micrography and X-ray mic-rotomography. Specific microcracking process was found to occur in this type of material. The occurrence of cracks was quantified and the morphology of the 3D crack network studied. The nature of the stitching yarn and the size of the diamond-shaped resin-rich regions were identified as having a major influence on laminate microcracking after ageing.

1. Introduction

Aircraft components are subjected to harsh time-dependent hygrothermal loadings during their service life. Those loadings are usually simulated by cyclical hygrothermal conditions in laboratories. The temperatures endured during aircraft service life can be as low as −55 °C and as high as 80 °C [1]. These cyclical temperature changes are known to induce residual stresses which may lead to crack initiation and growth in laminates, but these phenomena have only been observed in a few studies [1–6]. Chemical modification of the resin matrix is reported but only under steady loading and at higher temperatures [7–12]. Moreover, the epoxy resin which is used for aeronautics applications is known to have hydrophilic behaviour. The effect of water on composites has been studied under steady loading [8,13–16] and cyclical loading [17]. Some of the work on cyclical loading was done at cryogenic temperature (i.e. −196 °C) [18,19] which is far from service temperatures in aeronautics.

The specific morphology of polymer composites reinforced by Non-Crimp Fabric (NCF, Fig. 1a) requires to set up refined methodologies to characterise their durability, including the utilization of relevant accelerated cyclical tests. This raised the prospect of defining an experimental method to detect the interaction between the 3D morphology of NCF [20] and the hygrothermal microcracking process. The authors thus propose an accelerated testing and a method to characterise the local damage, adapted to the NCF laminates and to its multiscale heterogeneity, based on metallographic observations.

To characterise the interaction between the specific morphology of NCF and the cracks, 3D volumes of stitching areas were also studied by X-ray microtomography. It is shown that the method can give new information on the 3D network of cracks and be employed to validate the metallographic method.

To identify the influence of the type of stitching yarn used, interfaces between the stitching yarn and the polymer matrix were studied. Along this interface, sharp modification in the physical and mechanical properties takes place, which can lead to local microcracking, and the comparison of several types of stitching yarns can be relevant.

Overall, the objective here is to better understand and thus to reduce risks of microcracking in NCF materials during service life.

2. Problem of NCF durability

It is now well-known that the stitches in NCF laminates generate a complex morphology within the composite part, resulting in two main effects:

- firstly, local in-plane disorientations of the fibres occur in the vicinity of the stitches, those local disorientations create so-called "openings";
- secondly, they would generate two different types of resin-rich regions at the stitches (called "transverse channels") and at interplies because of the stitching yarn loop (called "interlayer gaps").

* Corresponding author. Tel.: +33 4 91 26 62 15.
E-mail address: pjliotier@gmail.com (P.-J. Liotier).

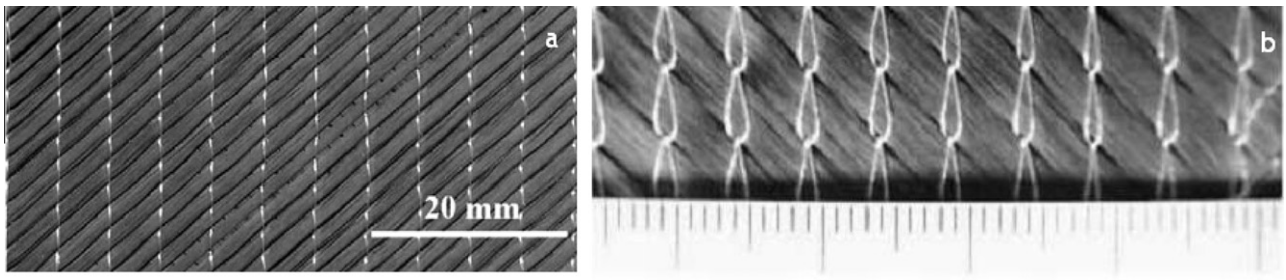

Fig. 1. NCF quadriaxial perform (a); NC2 quadriaxial preform (b) (stitching at 0°).

Several material and processing parameters control those effects, such as the geometry and the physical and mechanical properties of the stitching yarn, the density of the stitches and the stitching yarn tension [20].

The presence of stitching holes decreases the compactness in the preform and increases the permeability of it, which in turn basically controls the resin flow through the fibrous reinforcements during the injection or infusion process [21,22].

To improve the properties of these multiaxial materials and to minimize the resin-rich region sizes, novel types of reinforcements have been developed, among which the NC2® (Non-Crimp New Concept) (Fig. 1b) [20]. The main difference here is that the fibre yarns are first assembled in plies by using a thin hot melt yarn before the lamination process. These layers are cut, placed in the desired direction and then stitched together. It is worth noting that the stitching has no particular structural function and is useful to ease the handling and the processing of the multiaxials.

Fig. 1 shows that the stitches in the compact layers of NC2® do not lead to the formation of fibre rows with channels between them but only small diamond-shaped openings are still observable [21]. These openings have different sizes and shapes, according to the yarn size, the stitch type and the fibre orientation. They are of particular interest since they also serve as transverse channels to facilitate the resin flow when the preform is infused [22]. Finally they become resin-rich regions in the composite. The orientations of the two neighbouring stitched plies determines the direction of the diamond-shaped openings and thus of the three-dimensional periodic resin-rich regions inside the final laminate [23].

Laminate behaviour is thus affected by the morphology of the material at the meso level. The present study focuses on the influence of this specific morphology on material damage under hygrothermal cyclical loading.

A large number of studies on the durability of standard carbon reinforced materials have already been conducted, but no information is available in the literature on multiaxials. Studies focussing on resin modification in composites under humid loading have shown that complex phenomena may be involved during water saturation of the resin. Zhou and Lucas [8,16] indicate that the glass transition temperature continues to evolve after water saturation of the resin. Adams and Singh [13–15] showed that an irreversible plasticisation of the resin may occur after water saturation and drying of composite coupons. Moreover, the thermal loading effect on composites has been studied at high temperatures (140–150 °C), revealing that these temperatures induce resin oxidation at the surface of samples [9–12]. Epoxy resin has also been shown to be able to recombine at temperatures around 110 °C [8]. However, these temperatures are not directly related to service conditions in aeronautics and quite a few studies deal with the ageing of epoxy under lower temperatures. Montserrat et al. [7] found that structural relaxation can occur in an epoxy resin but still the conditions and mechanism should be clarified. Reynolds and McManus [1] showed that both hygrothermal and thermal cycles can induce resin microcracking in carbon reinforced laminates. Models of the microcracking of laminates subjected to thermal loadings have been developed [2,3], but these only consider the distances between consecutive cracks. None of the present models addresses the probability of crack initiation in unreinforced regions like resin-rich regions. Moreover, these models cannot take account of cyclical loading.

The rate of the temperature change also appears to have a significant incidence on the microcracking phenomenon. For instance, Ju and Morgan [24] studied the effect of thermal cycles with different temperature rates on the microcracking process in composites manufactured with prepregs, they concluded that 7 °C/min is more damaging than 2 °C/min.

3. Methods

3.1. Hygrothermal loading

The hygrothermal loading which is applied in this study is basically an adaptation of the cycles used by Klug [25] in his PhD work, which deals with the ageing of high-performance polymer adhesive systems. It is composed of a preliminary water absorption phase of 12 h at 50 °C and 95% HR followed by 400 pure thermal 1 h long cycles (Fig. 2). During each cycle, the testing temperature is maintained at 80 °C and −55 °C over periods of time of 15 min and the temperature rates are +9 °C/min and −9 °C/min to switch from one temperature to the other. The lower temperature is characteristic of temperatures recorded during a subsonic jet flight although the higher is regarded as the highest temperature aircraft structures might undergo in service (Fig. 2).

These types of cycles also induce steep water concentration gradient close to the surface of the coupons [17,26,27]. The coupons are 2 mm thick and placed inside an environmental chamber which provides mechanical heating/cooling and strong ventilation to ensure moisture homogeneity. The wet phase induces water saturation of the coupon surfaces while keeping constant low water concentration at the heart of the coupon. The thermal cycles dried the materials so that there is no water accumulation during the five loading groups of 400 cycles each. For this reason, the specimens were not dried before the test but only kept at equilibrium with ambient humidity corresponding to a uniform mass concentration of 0.015% of water.

The refined analysis of the damage close to the edges of the coupon is not straightforward because the water concentration gradient may induce stress concentration which depends on the anisotropy of the material. The amplitude of those gradients should be checked beforehand. An overestimation of the composite thickness affected by the gradient is obtained by assuming a Fickian behaviour along the fibres, whose diffusion coefficient is the highest. A simple calculation based on the one dimensional Fickian equation leads to a 5 mm region at the end of the water uptake phase.

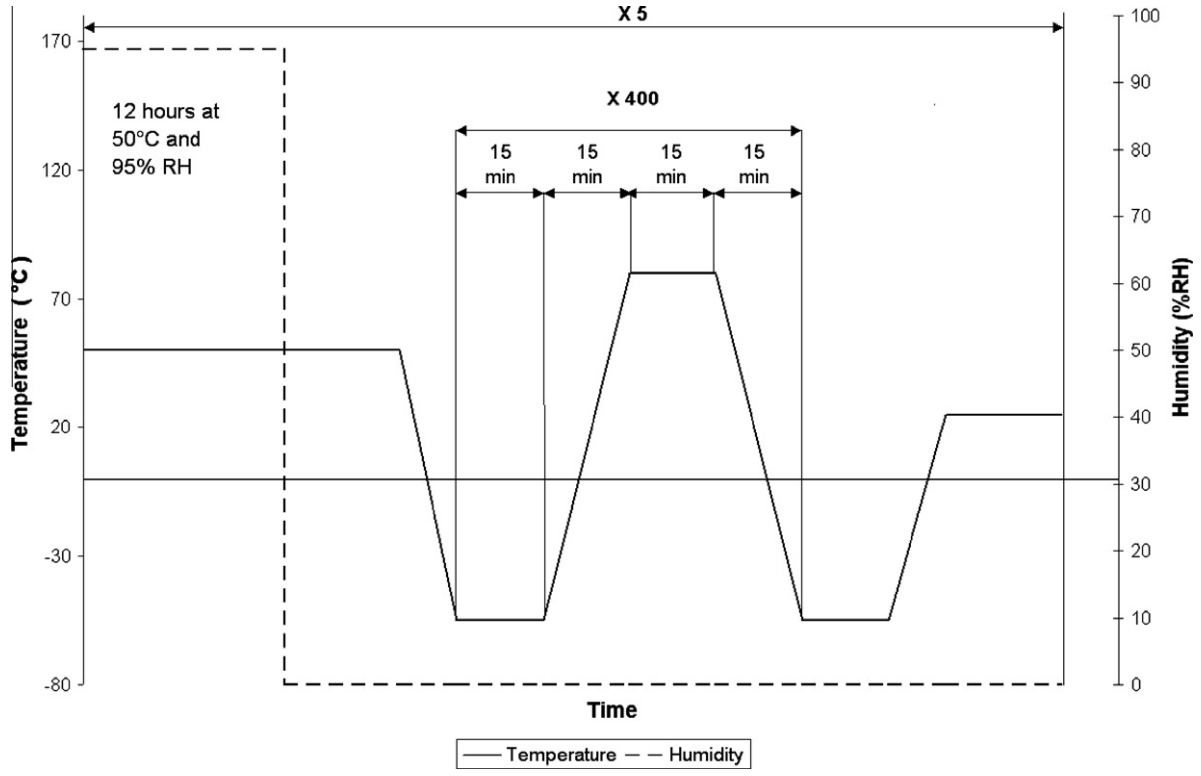

Fig. 2. Hygrothermal loading of 412.5 h.

3.2. Samples

The samples are cut from 30 × 30 cm^2 panels with a SiC rotative blade. These panels were manufactured by liquid resin infusion with RTM6® resin provided by Hexcel Corporation S.A.S. Note that the Hexcel Corp. Research and Development team also manufactured the panels, ensuring minimum internal defects. Reference coupons without any stitching, therefore without any resin-rich regions, were also supplied. These specimens comprise non-woven reinforcements, containing a negligible fibre volume fraction along the weft direction (Hexcel product/reference: G1157), and NC2®, whose stitching yarn has been removed. Thick stitching yarns have been used in order to sharpen the effect of the resin-rich regions. The particular effect of the yarn size on the resin-rich regions has been described in previous studies [20,26,28]. The nature of the stitching yarns has been selected beforehand to avoid any defects at the yarn/resin matrix interface. The yarns were manufactured from polyethylene terephtalate (PET), Novoloid®, which is a thermoset commercial resin, and polyamide (PA). PA/matrix interface appeared weaker than the other interfaces in a preliminary study. The yarn sizes are 76 dTex for the PET and PA yarns and 30 Tex for the Novoloid® yarns.

Since the resin-rich region shape is mainly relying on the ply stacking sequence, three different stacking sequences have been studied by using the Novoloid® stitched preform to assess the effect of the resin-rich region shape on sample microcracking.

Finally, a margin of 1 cm has been added to the 5 mm previously calculated and the region to be analyzed has been set to a 2 × 2 cm^2 square (Fig. 3). The minimum size of the coupon is 5 × 5 cm^2 whatever the thickness of the sample to ease the coupon handling and, to avoid experimental errors, a rectangular 5 × 6 cm^2 coupon has been finally selected. In Fig. 3 each node of the central grid figures a stitch. It is clear that there are two pairs of sections which are equivalent in terms of morphology and water concentration. The region of study contains nine stitches and 12 stitches located on the region edges can be analyzed. All the experiments have been performed with the rows of stitches running along the 5 cm edge.

The analyzed surfaces were located outside the central grid on the pieces named 1 and 2. We paired sections whose properties, hygrothermal stress and location relative to the stitch were similar to evaluate the scatter and ensure experimental consistency.

The surfaces were polished as previously described [20]. Mirror polishing allows to perform advanced observations of the sections and controlling abrasion during the polishing makes it possible to determine the location of the sections of interest with precision. Those sections were never located on a stitching row and the central piece of the coupon was systematically kept in case of accidental destruction of the initial section during polishing. Fig. 4 shows typical micrographs of a resin-rich region after cutting and polishing.

The analysis of the microcracking of a coupon after each loading group (i.e. a humid phase and 400 thermal cycles) requires a batch of five coupons of each type of material. After every 400 cycles, one coupon was cut out from the batch and used to characterise the microcracking of the resin. The crack characterisation method relied on optical observations after cross-section polishing (Figs. 4–7). Controlling abrasion during polishing makes it possible to select one or more stitches.

To reveal the effect of the humid phase, a 10 specimen batch was used, five specimens of which were not subjected to the humid period. These five specimens thus remained dry during the entire loading and are referred to as "dry". The five samples which have been fully conditioned are referred to as "wet".

4. Microcracking analysis

4.1. The problem

The classical approach to characterise the resin microcracking process of laminated composites is usually based on the observation

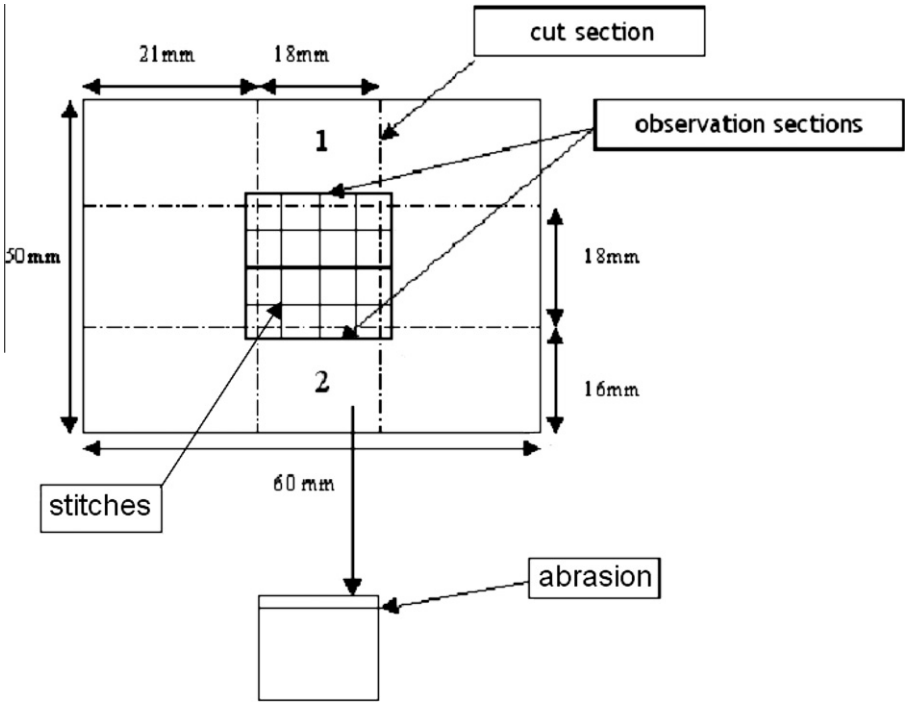

Fig. 3. Size of specimen tested and sample cut ($5 \times 6 \times 0.2\ cm^3$).

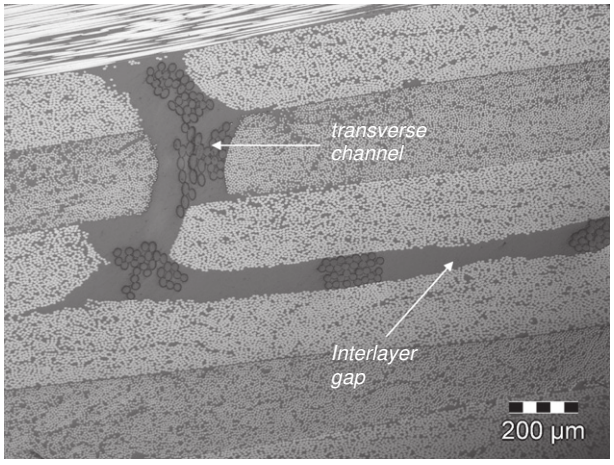

Fig. 4. Transverse channels and interlayer gaps with PA yarn.

of the specimen edges [1,18,19]. Reynolds and McManus [1] estimate the density of cracks of coupons in order to compare several types of damaging hygrothermal cycles. A single stacking sequence of composite made of prepregs was tested: $[90/90/0/0/0/0/90/90]_S$. Samples thus had 4 UD plies at 90° at its centre.

The study compare two different hygrothermal cycles:

- the baseline cycle: two dry stages at 163 °C and −54 °C and a wet stage at 87 °C and 85% relative humidity for a duration of 160 min/cycle;
- an accelerated cycle: two dry stages at 163 °C and −54 °C and a wet stage at 87 °C and 85% relative humidity for a duration of 90 min/cycle.

The determination of the crack density in the central 90° plies is based on the micrographic optical observations of the two opposite edges of each specimen which used to be mirror-polished before environmental conditioning. The authors are thus able to focus on the emerging cracks. It is important to notice that the authors do not take into account cracks in the external 90° plies, although no explanation is given for this.

The main conclusion the authors draw is that the cracks in the four 90° inner plies used to move from one interply to another, therefore they define four families of cracks depending on the number of interplies which are affected: cracks going through one single ply (referred to as f_1), going through 2 plies (referred

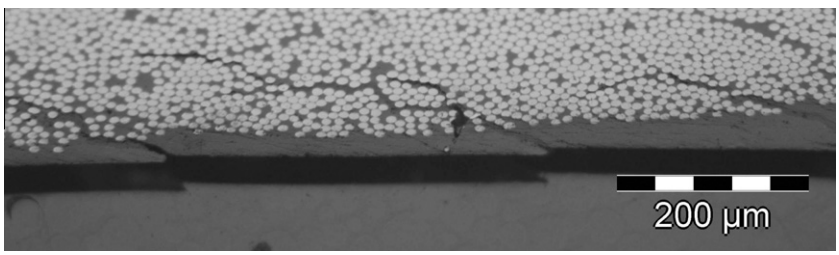

Fig. 5. Cracks at the edges in outer plies in unstitched laminates.

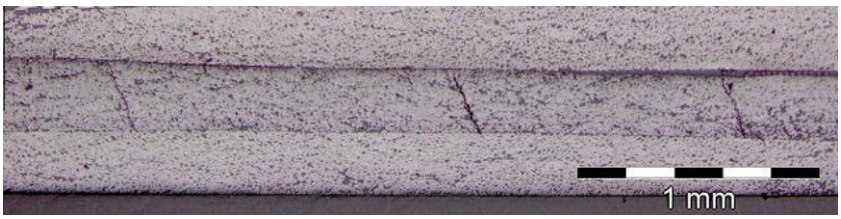

Fig. 6. Cracks at the edge in inner plies in unstitched laminates. (For interpretation of the references to colour in this figure legend, the reader is referred to the web version of this article.)

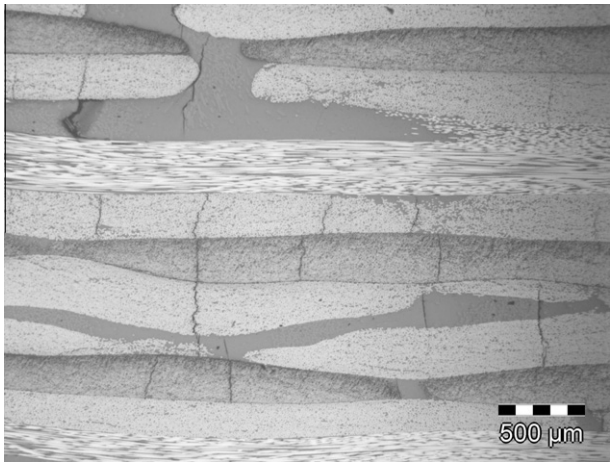

Fig. 7. Inner cracks with Novoloid® yarn in quasi-isotropic laminates.

to as f_2), going through 3 plies (referred to as f_3) and going through 4 plies (referred to as f_4).

The crack density criterion based on this classification can be written as follows:

$$d_c = \frac{4f_4 + 3f_3 + 2f_2 + f_1}{NnL}$$

where N is the number of specimens, n is the number of observed edges for each sample and L is the effective sample length observed. The crack density is expressed in cracks by edge by cm. This makes the crack density value reliable but does not allow any characterisation of dispersion along the different edges. Moreover, it is assumed that the effective length L is long enough to ensure that the density d_c is an intrinsic parameter which characterises the state of damage of the specimen.

The authors observed the specimens after each block of 500 cycles and characterise the cracks which go through the four central plies. They find that for the f_4 cracks, the baseline cycle leads to earlier crack onset and higher crack density. These cracks are observable only after 2000 cycles of the accelerated loading and the estimated crack density does not exceed 2 cm^{-1}. The study shows that monitoring the hygrothermal cracking process is possible with this method. However, the characterisation of the cracks occurring on the edge of the specimens raises the question of a possible influence of the moisture gradients on the data, this explains our present decision of cutting out the specimen to have a look inside.

4.2. Defining a reliable criterion

Fig. 7 clearly shows that inner ply cracks within the specimen are oriented along the specimen thickness, although outer ply cracks at the specimen free edge are inclined (Fig. 5). For a quasi-isotropic laminate the angle of the cracks with the interply tends to $20 \pm 2^\circ$ and cracks appear to be concentrated in the same ply (Fig. 6). This could be related to the complex stress gradients due to water concentration close to the free edge of the specimen. These gradients become complex near the free edge because of the different hygrothermal strains of the plies which finally result in local hygrothermal residual stresses.

The conclusion drawn from the study of the specimen free edge microcracking is that crack characterisation is really a difficult task for usual stacking sequences because of mechanical state which is not completely under control. In addition, the presence of stitches on the edge of the sample induces even more complex local stress gradients. This justifies our choice to characterise the microcracking in the central zone of the sample where no free edge effect ise acting.

It is impossible to approach a 3D crack network from the observation of a section. For instance, two cracks which look as completely independent in two consecutive plies in one given observation plane can merge into one single crack in another plane because they can propagate along the fibre directions of the two plies. Thus, when counting the number of cracks in a section, it is necessary to take into account the number of plies that every crack crosses.

In order to be able to compare several multiaxials, the criterion should be independent of any stacking sequence. Thus, the number of cracks in each ply should be considered. The number of plies only includes the plies where the cracks can be detected; Therefore, plies whose fibres are parallel to the cutting edge are not taken into account.

Finally, the criterion can be written as follows, for the observation of N_i cracks in ply number i of a laminate with p plies, where cracks can be detected along the length L:

$$d = \frac{\sum_i N_i}{Lp}$$

p is the number of plies where cracks can be detected, that is the total number of plies excluding the plies parallel to the observation plane. Cracks in resin-rich regions and cracks within the plies of the laminate are not distinguished.

L is a critical parameter, it is designed to permit the observation of a minimum of three resin-rich regions (i.e. 15 mm) and so it takes account of the microcracking scatter. It is assumed that the d parameter is intrinsic to the material under the hygrothermal loading considered.

5. Results and discussion

5.1. Test on unstitched laminates

To validate the method on standard laminates without stitching, we performed tests on two types of reinforcements: firstly a woven material with a negligible quantity of fibres in the weft direction and unstitched NC2® and secondly a quasi-isotropic ($[135/0/45/90]_S$) laminate. These laminates are manufactured by liquid resin infusion and since the yarns have been removed, the

Table 1
Crack densities in non-stitched laminates.

Material type	Crack density d (cm^{-1})				
	400 cycles	800 cycles	1200 cycles	1600 cycles	2000 cycles
Dry weave	0 ± 0	0 ± 0	0 ± 0	0 ± 0	0.2 ± 0.0
Wet weave	0 ± 0	0 ± 0	0 ± 0	0 ± 0	0.2 ± 0.1
Dry unstitched NC2®	0 ± 0	0.05 ± 0.05	0 ± 0	0 ± 0	0.4 ± 0.1
Wet unstitched NC2®	0 ± 0	0 ± 0	0 ± 0	0 ± 0	0 ± 0

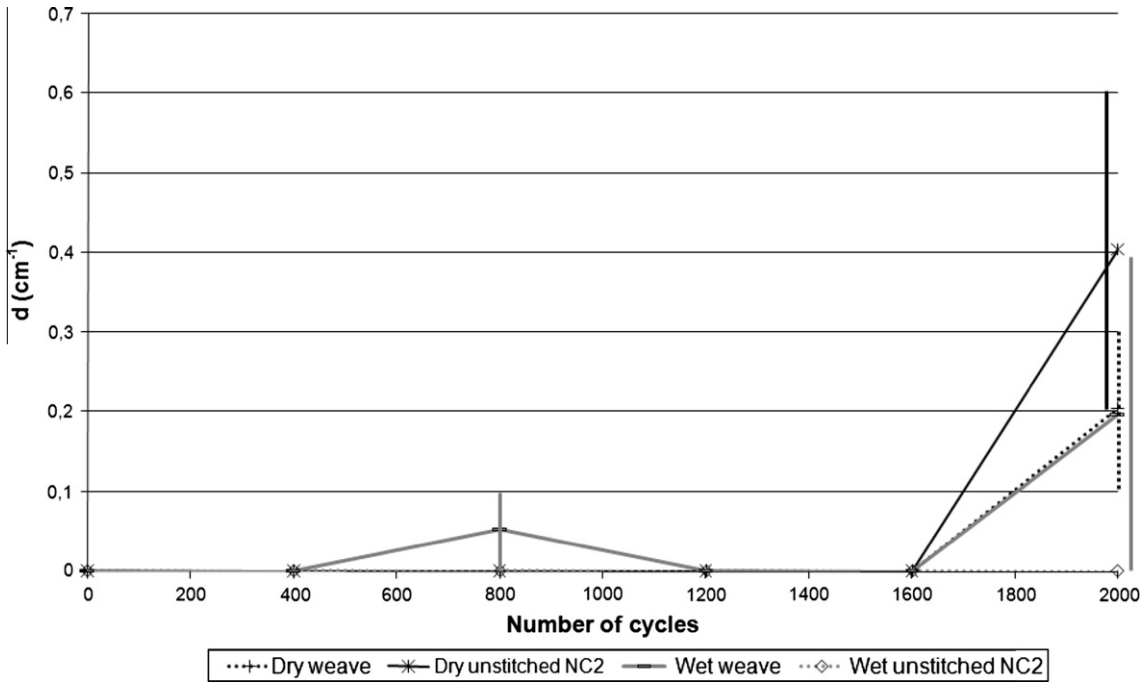

Fig. 8. Crack density d versus the number of cycles for unstiched laminates.

fibres can move during processing and the diamond-shaped openings disappear. Direct observations confirm that no resin-rich region occurs in these laminates.

The evolution of the crack density (and the associated dispersion) estimated using the method discussed in Section 4.2 is reported in Table 1. Fig. 8 shows the crack density measured after 400, 800, 1200, 1600 and 2000 cycles. The vertical lines represents the range from maximum to minimum values between the two opposite sections shown in Fig. 3.

The characterisation of the microcracking of unstitched laminates under hygrothermal loading showed that thermal fatigue ageing is significant after 2000 thermal cycles and thus confirms first results of the literature [1], even though the loading, the processing and stacking sequences are different. The lower temperature which is the same as that in the literature appears to be an essential parameter of hygrothermal loading.

Conclusions on the effect of the humid conditioning of the wet specimens can also be drawn from these tests. This effect is weak on the woven material and cannot be detected on unstitched NC2®. The dry sample was expected to show a higher crack density because of the lowering of stress due to hygroscopic swelling in wet samples. However, experimental results do not confirm such a trend for these materials, one reason might be that the water concentration within the material was not sufficient to lead to any detectable changes.

5.2. Evolution of microcracking on stitched cross-ply laminates

The choice of focussing first on the specific properties of this material, by achieving large resin-rich regions in the sample tested (Novoloid® 30 Tex yarns, refer to Liotier et al. [20] for the description of the particular morphology due to this yarn), have been made. Moreover, to simplify the characterisation of the cracking paths, two cross-ply laminates have been selected: $[90/0/0/90]_S$ and $[135/45/45/135]_S$ laminates, whose stitching row is oriented at 0° and plies are stitched four by four. The crack density and the associated dispersion at different loading times are shown in Fig. 9 (Table 2). We treated two series of samples: the first was subjected to the full hygrothermal loading and labelled "wet" and the second subjected to the thermal cycles only and labelled "dry" (Fig. 9). Fig. 9 shows the crack density measured after 400, 800, 1200, 1600 and 2000 cycles. No significant difference can be detected between the crack densities of the dry and wet specimens, meaning that the moisture conditioning which has been performed is not so critical. This conclusion is even more obvious from Fig. 9.

If the two materials are compared, it appears that the $[135/45/45/135]_S$ laminate tends to produce a lower crack density than the $[90/0/0/90]_S$ laminate. The second reached around 3.5 cracks/cm/ply while the first reached around 2.5 cracks/cm/ply.

This is due to the inner morphology of the material: in the $[90/0/0/90]_S$ laminate, the resin-rich regions are connected with each

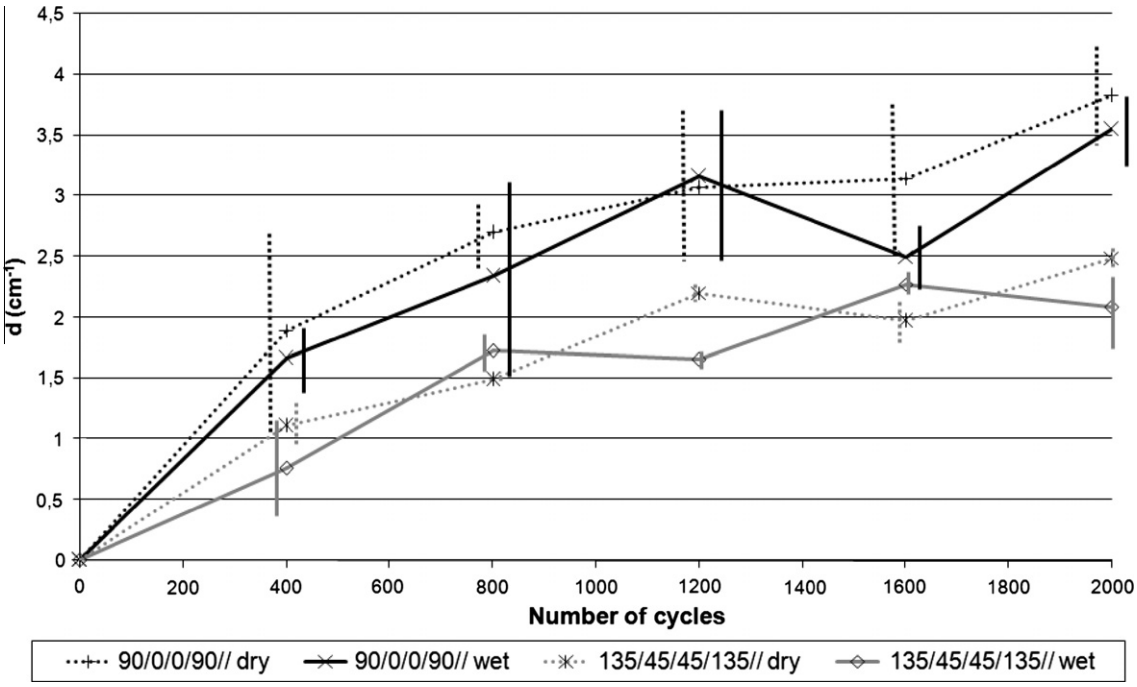

Fig. 9. Crack density d versus the number of cycles for cross ply multiaxial stitched preform.

Table 2
Crack densities in cross ply multiaxials with Novoloid® yarns.

Material type	Crack density d (cm^{-1})				
	400 cycles	800 cycles	1200 cycles	1600 cycles	2000 cycles
$[0/90/90/0]_2$ dry	1.9 ± 1.1	2.7 ± 0.3	3.1 ± 0.7	3.1 ± 0.6	3.8 ± 0.4
$[0/90/90/0]_2$ wet	1.7 ± 0.2	2.3 ± 0.9	3.2 ± 0.5	2.5 ± 0.1	3.5 ± 0.3
$[135/45/45/135]_S$ dry	1.1 ± 0.2	1.5 ± 0.1	2.2 ± 0.1	2.0 ± 0.2	2.5 ± 0.1
$[135/45/45/135]_S$ wet	0.8 ± 0.4	1.7 ± 0.2	1.7 ± 0.0	2.3 ± 0.1	2.1 ± 0.3

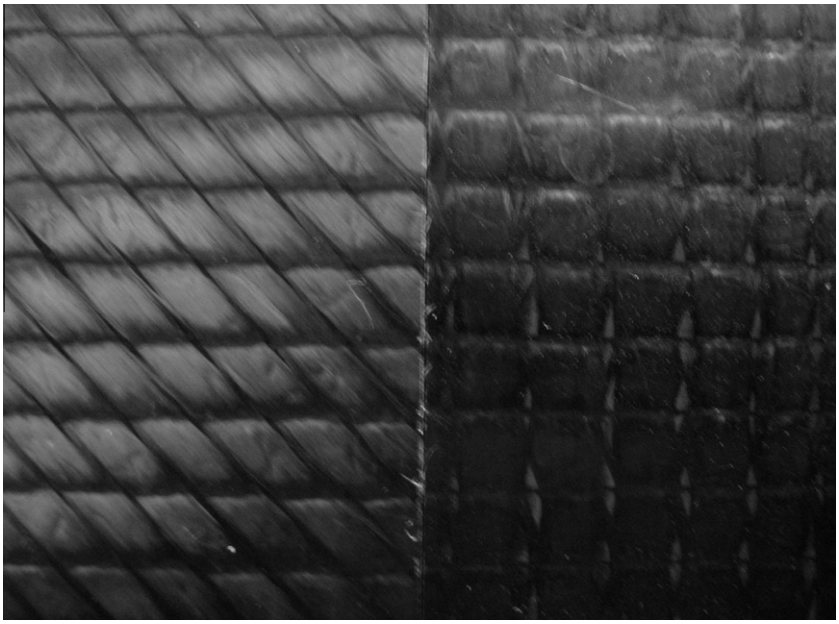

Fig. 10. Effects of stitching direction.

other (resin channels in the ply), while the resin-rich regions of the second laminate are smaller and are not connected (Fig. 10). The difference in behaviour under hygrothermal loading can be attributed to this morphological difference.

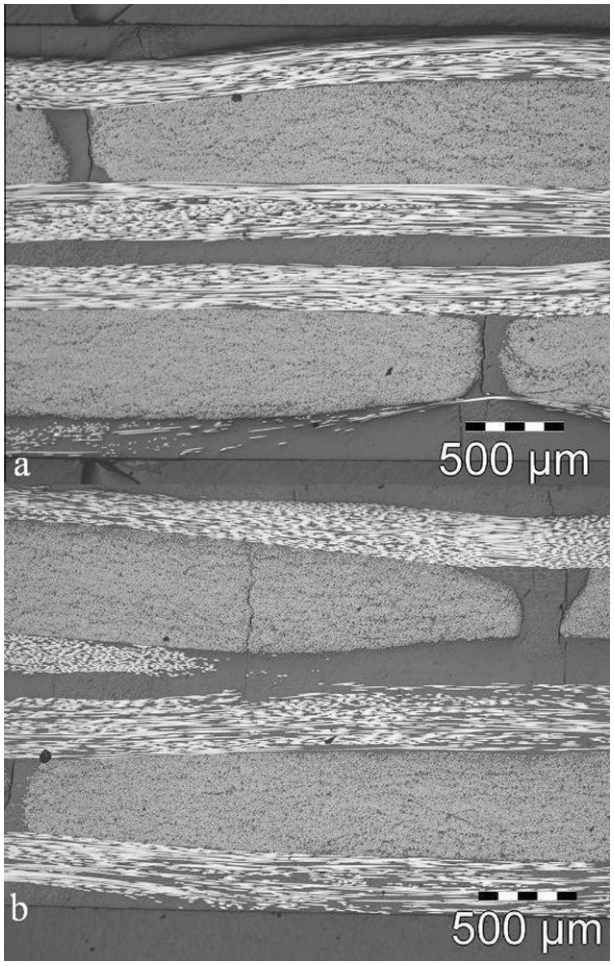

Fig. 11. Crack location versus the number of cycles in biaxial laminates with Novoloid® yarns: (a) 1200 cycles, (b) 2000 cycles.

The other interesting results lie in the crack locations. For the $[90/0/0/90]_S$, the short ageing time produces cracks located in the resin-rich regions near the stitching yarn (from 400 cycles to 1200 cycles). In the specimens subjected to more than 1200 cycles, cracks in within the laminate plies can be found as well. Fig. 11 shows that cracks occur in plies after the full hygrothermal loading. The occurrence of these cracks in both stitched and unstitched laminates is obtained for a similar number of cycles. In conclusion, it seems that there are two different microcracking modes; one being very specific to the stitched composites and which occurs in resin-rich regions only, and another one which is common to all composite laminates (herein called transverse microcracking) [28].

To confirm the morphological effect and to study the two microcracking modes, 3D investigations were performed on quadriaxial stitched laminates.

5.3. Evolution of microcracking in stitched quadriaxial laminates

In a stitched quadriaxial laminate with Novoloid® 30 Tex yarns, the resin-rich regions have a complex 3D shape [20] that can lead to crack reorientation. Crack propagation in quadriaxial quasi-isotropic laminates is known [19] to cause delamination before the cracks cross from one ply to another with a different fibre orientation. Here, three-dimensional crack networks without delaminated zones have been observed.

Crack density evolves erratically, as shown in Fig. 12, where the *d* parameter apparently decreases when the number of cycles increases (Table 3). Fig. 12 shows the crack density measured after 400, 800, 1200, 1600 and 2000 cycles. The scatter could be caused by the uncertainty on the position of the observation plane or by the non-repeatability of crack propagation through a material whose microstructure is highly complex. The first hypothesis has been investigated by 3D characterisation using X-ray microtomography.

5.4. 3D microcrack network in quadriaxial laminates

The microcracking of the resin-rich region used to lead to complex crack network. The 3D description of those networks can be approached by X-ray microtomography [20,26].

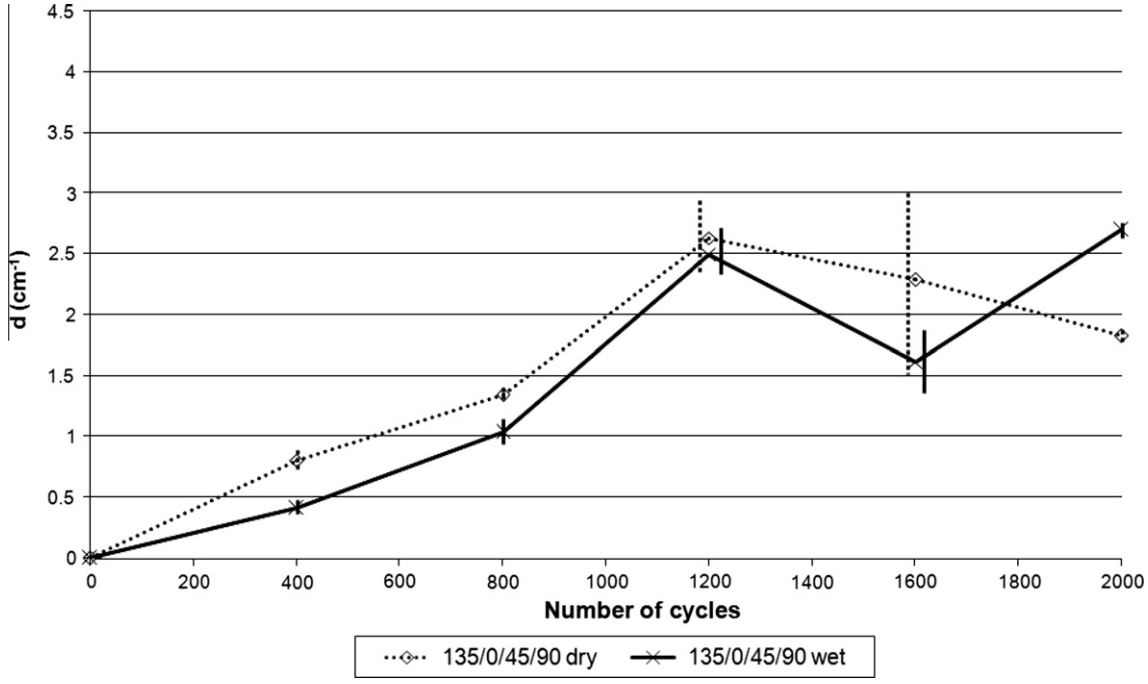

Fig. 12. Crack density versus the number of cycles for quasi-isotropic laminates.

Table 3
Crack densities in quasi-isotropic multiaxials with Novoloid® yarns.

Material type	Crack density d (cm^{-1})				
	400 cycles	800 cycles	1200 cycles	1600 cycles	2000 cycles
$[135/0/45/90]_S$ dry	0.8 ± 0.1	1.3 ± 0.1	2.6 ± 0.3	2.3 ± 0.3	1.8 ± 0.1
$[135/0/45/90]_S$ wet	0.4 ± 0.2	1.0 ± 0.3	2.5 ± 0.2	1.6 ± 0.2	2.7 ± 0.1

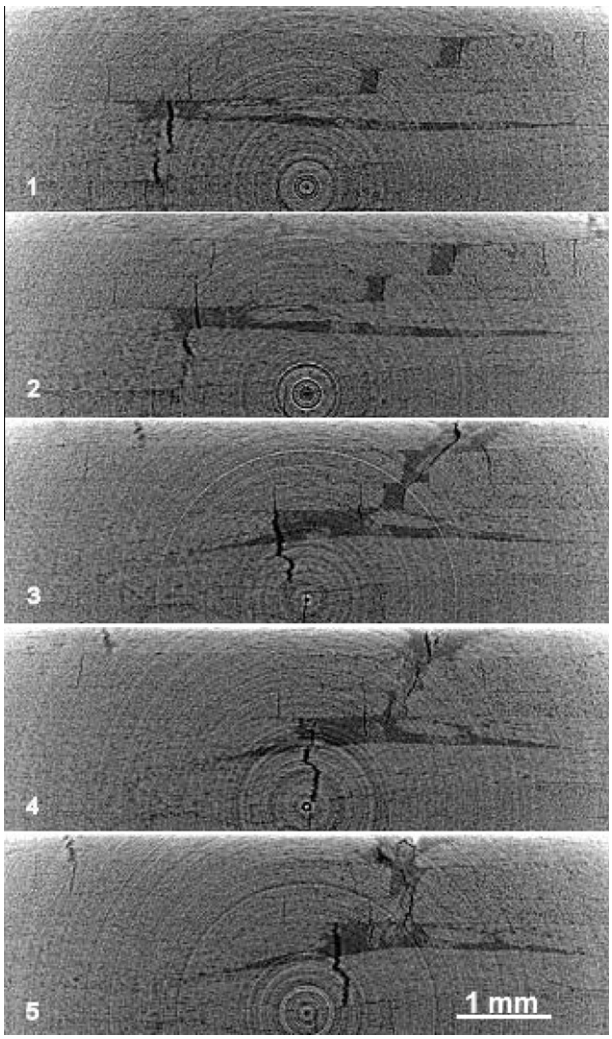

Fig. 13. 3D exploration of a resin-rich region part 1.

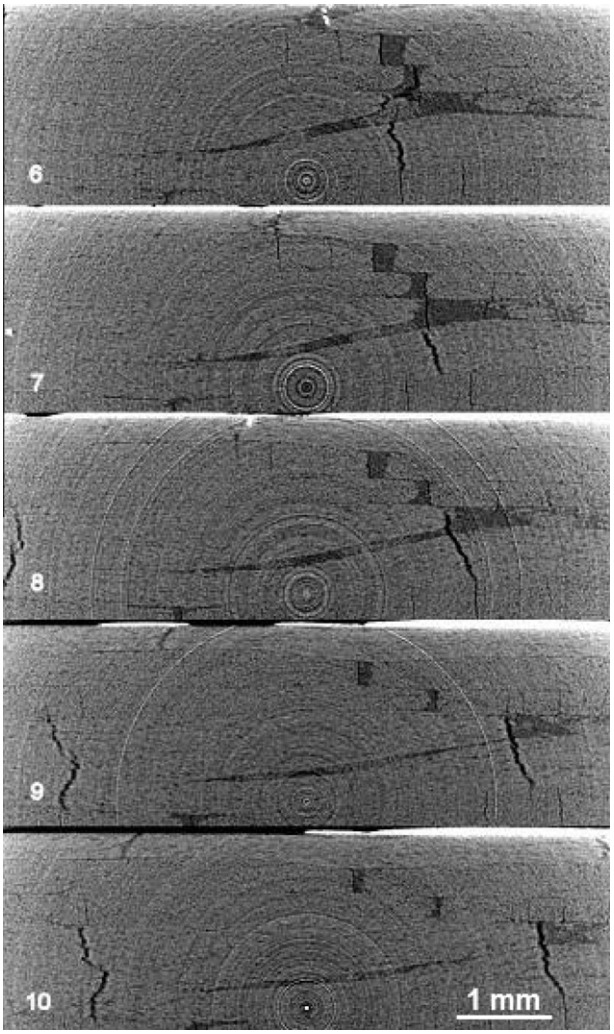

Fig. 14. 3D exploration of a resin-rich region part 2.

The quasi-isotropic laminates with PET stitching yarn were subjected to the full hygrothermal loading, i.e. 2000 hygrothermal cycles and five humid stages. Figs. 13 and 14 present sections of a 3D volume, which is schematically shown in Fig. 15. The voxel size of $2.5 \times 2.5 \times 2.5\ \mu m^3$ and the volume is composed of $1290 \times 600 \times 360$ voxels.

The sections shown in Figs. 13 and 14 are not separated by a constant offset of voxels, but they were chosen to show a typical crack distribution. The cracks in those selected sections move from one ply to another.

By comparing the crack density of different sections of the resin-rich regions, it is possible to obtain an estimate of the scatter due to the uncertainty of the experimental observation, and thus determine whether the erratic evolution of the crack density in quasi-isotropic laminates can be simply explained by the variability in the cross-section locations due to the abrasion process of the specimen polishing.

Crack density of the 10 sections in Figs. 13 and 14 is characterised (Table 4). They show that uncertainty on the plane position does not explain the erratic evolution of the crack density detected in Section 5.3. Therefore, the apparent highly erratic data should be caused by the non-repeatability of the microcracking phenomenon.

These volumes reveal how cracks propagate outside the resin-rich regions. Cracks can be observed beyond the extremities of the diamond-shaped resin-rich regions and can extend through the entire multi-ply stack thickness within the transverse channel. In each ply the crack changes its direction, propagating along the fibres (Fig. 16).

We can thus conclude that conditions in the resin-rich regions allow cracks both to cross from one ply to another and to change

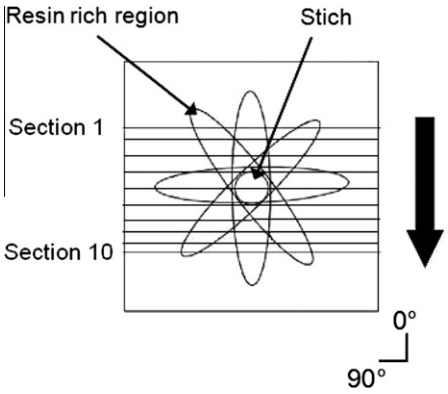

Fig. 15. Analyzed cross-sections in the resin-rich region.

Table 4
Local crack densities on several sections of a single PA stitch.

Section N°	Number of cracks	Local crack density cracks/cm/pli
1	12	0.50
2	11	0.46
3	13	0.54
4	12	0.50
5	14	0.59
6	12	0.50
7	12	0.50
8	12	0.50
9	13	0.54
10	13	0.54

their direction of propagation as well. Moreover, the cracks are not limited to the resin-rich region and can propagate in the plies. This conclusion is of major importance, as this type of crack has never before been observed in NCF microcracking [29,30].

Furthermore, Figs. 13, 14 and 16 show that the cracks often propagate at the interface between the plies and the resin-rich regions, which is in agreement with the fact this transition zone is highly heterogeneous at the mesoscopic scale in terms of mechanical and physical properties, and thus undergoes stress concentration during the thermal loading.

Another main conclusion of this work is the existence of two types of microcracks. The two crack networks and their connectivity can be observed by X-ray microtomography. To understand the morphology of the two crack networks, projections of the darkest grey of the volume transverse to the ply direction were made. Fig. 17 shows a projection perpendicular to the ply plane of the lightest grey of the area in Figs. 13 and 14.

Fig. 17 shows the relative location of the cracks inside the resin-rich regions and it can be observed that the cracks cross over in the stitching yarn, changing their direction to follow the fibres. Cracks of the second type can be identified because they are independent of the resin-rich regions.

Combining observations of Figs. 13, 14 and 17, it appears that the second type of cracks is not long enough to be connected to each other but they seem to be systematically connected to cracks from the first microcracking process in a different ply. These second-type cracks may, thus, either be propagated directly from the first type, or else be favoured by conditions induced by the preceding crack.

5.5. Effects on the yarn/matrix interface

Interfaces between stitching yarns and polymer matrix can be observed by Scanning Electron Microscopy (SEM). A JSM 6400

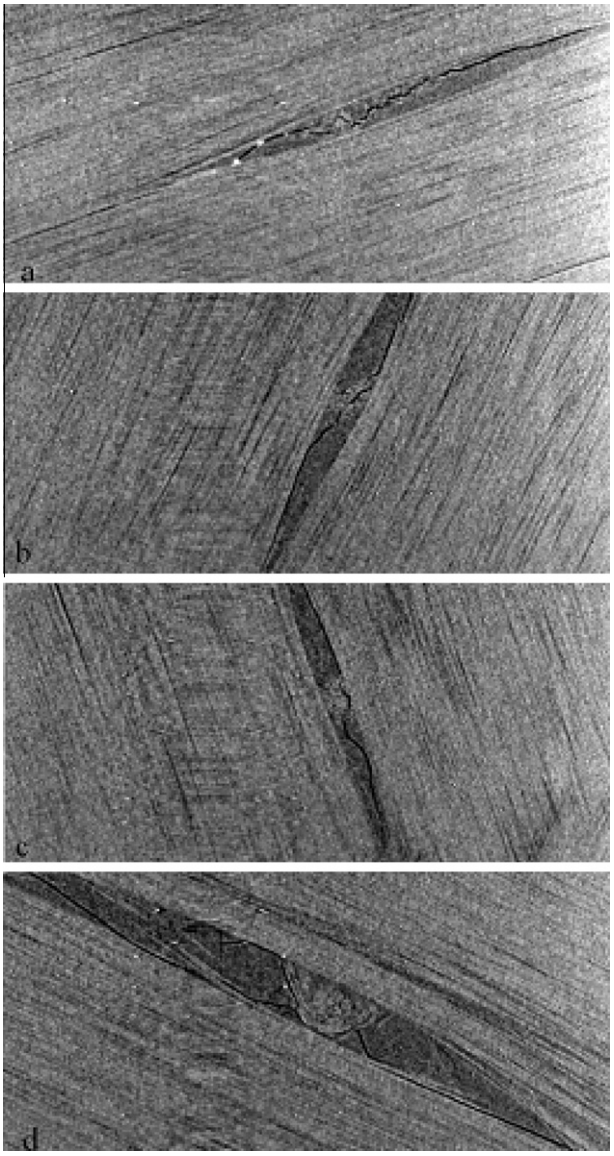

Fig. 16. Microcrack propagation in the transverse channel.

has been used to perform the observations. The samples are polished to mirror state and covered by a micrometric coat of gold/palladium by cathodic pulverisation. This allows the observation of micro-delamination between the yarn and the polymer matrix without any charging effect due to the localised electron beam.

SEM images show the different constituents of the material in greys with weak contrast. The carbon fibres and the stitching yarns are identified by surface texturing. This method was chosen to study the interface because it allows a better resolution than optical observation and avoids the problems of shadows or light scattering. Fig. 18 is an observation of an virgin specimen.

It is clear that the yarn/polymer matrix interface remains intact. After 400 thermal cycles, microcracks appear at the interface between yarn and matrix. These microcracks can be characterised by a smaller opening than previous ones (Fig. 19). They may cause crack initiation or propagation.

Tests were performed on three types of stitching: PolyAmide (PA), PET and Novoloid® to identify their particular sensitivity to hygrothermal loading. None of the virgin samples shows any damage, even with large magnification (Fig. 20). We thus conclude that the coupon preparation does not induce significant damage. Let us

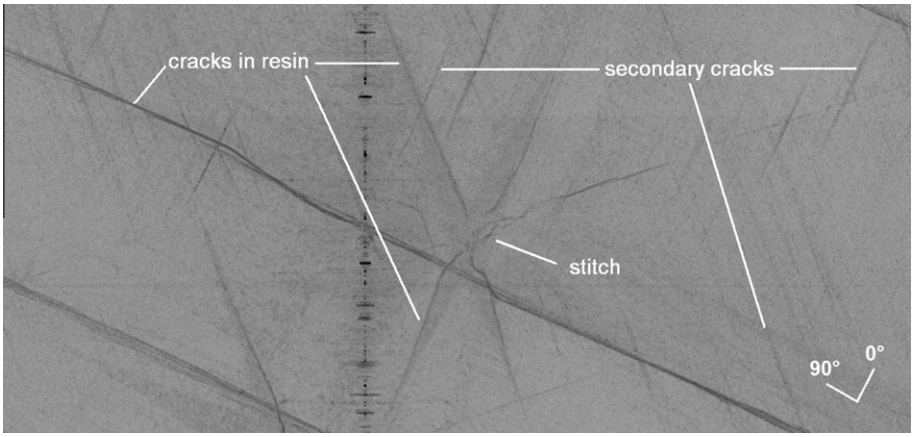

Fig. 17. Projection of the darkest grey and discussion.

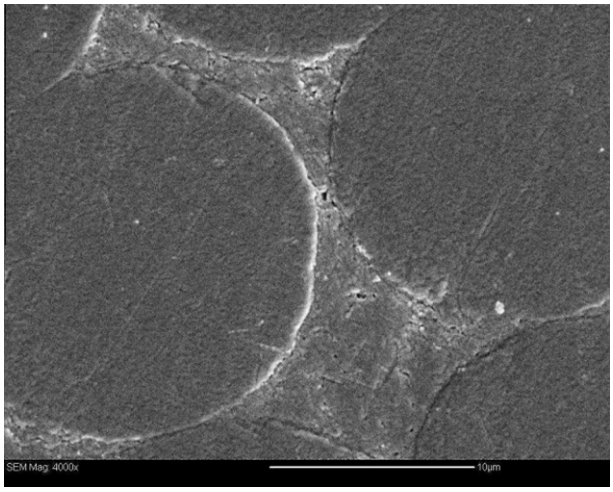

Fig. 18. Non-aged resin/PA yarn interface obtained by SEM (4000×).

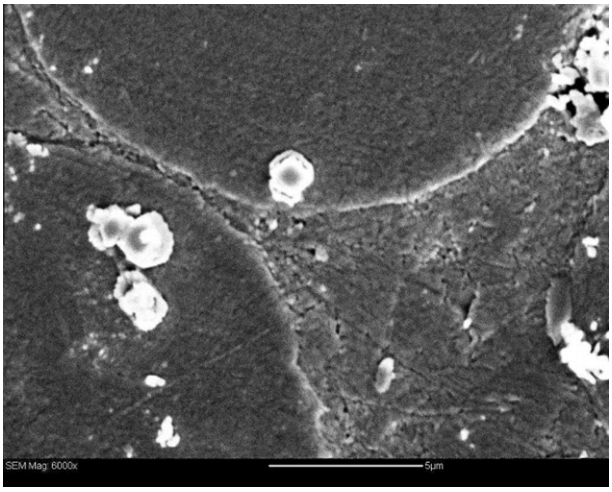

Fig. 20. Non-aged specimen with PA yarns (6000×).

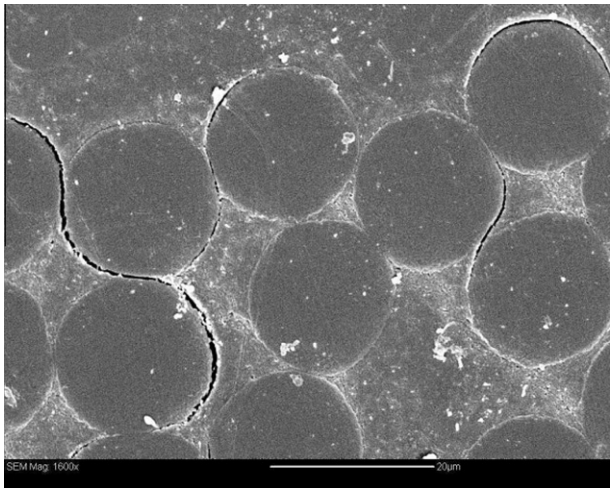

Fig. 19. Damaged resin/PA yarn interface after hygrothermal loading.

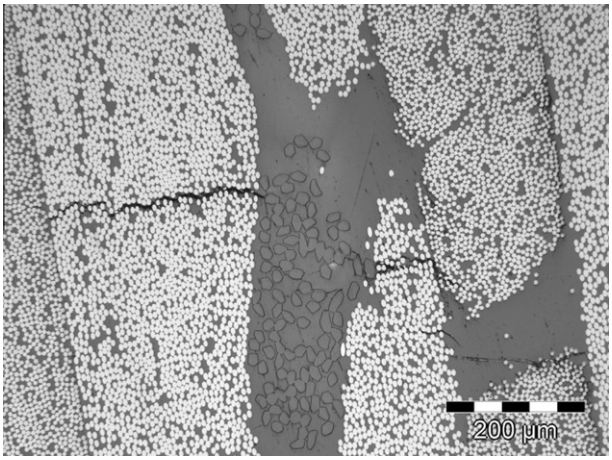

Fig. 21. Crack propagation in resin/PE yarn interface.

point out that the stitching areas are sometimes difficult to detect because of the low grey contrast between the materials; to facilitate the observation, it is possible to mark the coupon with a thin felt-tip marker.

The Novoloid® yarns are still undetectable with the gold/palladium coating. The PA yarns show cracks in the interface between stitching yarns and matrix (Fig. 19). The PET yarns are the only ones whose yarn/polymer matrix interfaces remain intact after hygrothermal loading. However, it is important to note that even

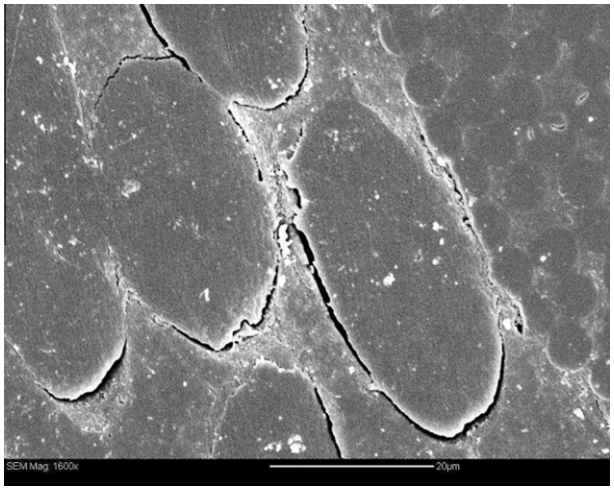

Fig. 22. Damaged interface on PA yarn after ageing.

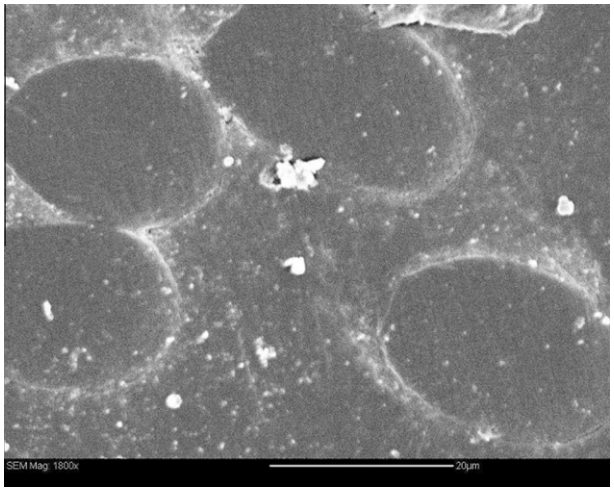

Fig. 23. Non-damaged PA yarn in the interlayer gaps after ageing.

though the PET yarns do not show deterioration of the interface at a distance from the bigger cracks, this interface appears to be a preferred path for crack propagation (Fig. 21).

Interface microcracking was not detected with Novoloid® yarns. Optical observations show that the crack goes through the yarn itself rather than across the yarn/matrix interface. We thus conclude that the nature of the Novoloid® yarn produces a strong interface which can sustain residual thermal stresses.

Another important conclusion can be drawn from observations of the PA yarn. Interface microcracking is rare in the stitching yarn loops even after the full loading cycle. Yarn/matrix interface microcracks are systematic in the transverse channels (Fig. 22) but not in the interlayer gaps (Fig. 23). These findings should help select yarns according to their ability to delay the onset of cracks and to limit their propagation.

6. Conclusion

The durability of composites reinforced by stitched multiaxial stacks was investigated by implementing thermal cyclical loading with or without preliminary humid conditioning. A specific method of coupon preparation and polishing was developed to reduce artefacts and allow to characterise the stitching areas where resin-rich regions are located. The main results can be summarised as follows:

- specific cracks occur within the resin transverse channels surrounding the stitches, showing that hygrothermal damage is different to that caused by mechanical loading [30];
- the humid phase of the hygrothermal loading tested does not show any significant and detectable effect;
- the size of the resin-rich regions appears to be a critical factor in crack density at the end of thermal cycling;
- 2D observations combined with 3D network crack characterisation finally show that microcracking repeatability is not sufficient for it to be studied in 2D.

Here, defining a method of detecting microcracks at the interface between the stitching yarn and the polymer matrix made it possible to characterise the effect of the type of yarn used. This reveals that the nature of the yarn has a significant influence, and that PA yarn for instance is not a judicious choice.

These results open the way to developing a stitched multiaxial reinforcement which avoids microcracking inside the resin-rich regions, through reducing resin-rich regions as far as possible and improving yarn/matrix toughness.

Acknowledgments

The authors are grateful to Christine Délisée, Jérôme Malvestio and the USBB for the X-ray microtomographic 3D images. We thank Marjorie Sweetko for help with the English of the manuscript.

References

[1] Reynolds TG, McManus HL. Accelerated tests of environmental degradation in composites materials, composites structures: theory and practice. ASTM STP 1383. In: Grand P, Rousseau CQ, editors. West Conshohocken, PA: American Society for Testing and Materials; 2000. p. 513–25.
[2] Park CH, MacManus HL. Thermally induced damage in composite laminates: predictive methodology and experimental investigation. Compos Sci Technol 1996;56:1209–19.
[3] Nickerson S, Mayes JS, Welsh JS. Multi-continuum analysis of thermally induced matrix cracking. Eng Fract Mech 2005;72:1993–2008.
[4] Givler RC, Gillespie JW. Environmental exposure of carbon/epoxy composite material systems, composites for extreme environments. ASTM STP 768. In: Adsit NR, editor. American Society for Testing and Materials; 1982. p. 137–47.
[5] Delasi R, Whiteside JB. Effect of moisture on epoxy resins and composites, advanced composite materials-environmental effects. ASTM STP 658. In: Vinson JR, editor. American Society for Testing and Materials; 1978. p. 2–20.
[6] Collings TA, Stone DEW. Hygrothermal effects in CFRP laminates: strains induced by temperature and moisture. Composites 1985;16(4):307–16.
[7] Montserrat S, Gomez Ribelles JL, Meseguer JM. The application of a new configurational entropy model to the structural relaxation in an epoxy resin. Polymer 1998;39:3801–7.
[8] Zhou J, Lucas JP. Hygrothermal effects of epoxy resin. Part I: the nature of water in epoxy. Polymer 1999;40:5505–12.
[9] Drukker E, Green AK, Marom G. Mechanical and chemical consequences of through thickness thermal gradients in polyimide matrix composite materials. Composite: Part A 2003;34:125–33.
[10] Hancox NL. Thermal effects on polymer matrix composites: part 1. Thermal cycling. Mater Des 1998;19:85–91.
[11] Lafarie-Frenot MC, Rouquié S, Ho NQ, Bellenger V. Comparison of damage development in C/epoxy laminates during isothermal ageing and thermal cycling. Composite: Part A 2006;37:662–71.
[12] Rouquie S, Lafarie-Frenot MC, Cinquin J, Colombaro AM. Thermal cycling of carbon/epoxy laminates in neutral and oxidative environments. Compos Sci Technol 2005;65:403–9.
[13] Lin YC, Chen X. Moisture sorption-desorption-resorption characteristics and its effect on the mechanical behavior of the epoxy system. Polymer 2005;46:11994–2003.
[14] Singh MM, Adams RD. The dynamic properties of fibre-reinforced polymers exposed to hot, wet conditions. Compos Sci Technol 1996;56:977–97.
[15] Singh MM, Adams RD. Low temperature transitions in fibre reinforced polymers. Composite: Part A 2001;32:797–814.
[16] Zhou J, Lucas JP. Hygrothermal effects of epoxy resin. Part II: variation of glass transition temperature. Polymer 1999;40:5513–22.

[17] Jedidi J, Jacquemin F, Vautrin A. Accelerated hygrothermal cyclical tests for carbon/epoxy laminates. Composite: Part A 2006;37(4):636–45.
[18] Kim RY, Donaldson SL. Experimental and analytical studies on the damage initiation in composite laminates at cryogenic temperatures. Compos Struct 2006;761(2):62–6.
[19] Bechel VT, Kim RY. Damage trends in cryogenically cycled carbon/polymer composites. Compos Sci Technol 2004;64(12):1773–84.
[20] Liotier PJ, Vautrin A, Delisée C. 3D Morphological characterization and microcracks detection in composites reinforced by multiaxial multiply stitched preform. Composite: Part A 2010;41:653–62.
[21] Lomov SV, Belov EB, Bischoff T, Ghosh SB, Truong Chi T, Verpoest I. Carbon composites based on multiaxial multiply stitched preforms. Part 1: geometry of the preform. Composite: Part A 2002;33:1171–83.
[22] Drapier S, Pagot A, Vautrin A, Henrat P. Influence of the stitching density on the transverse permeability of non-crimped new concept (NC2) multiaxial reinforcements: measurements and predictions. Compos Sci Technol 2002;62(15):1979–91.
[23] Chun HJ, Kim HW, Byun JH. Effects of through-the-thickness stitches on the elastic behaviour of multi-axial warp knit fabric composites. Compos Struct 2006;74:484–94.
[24] Ju J, Morgan RJ. Characterization of microcrack development in bmi-carbon fibre composite under stress and thermal cycling. J Compos Mater 2004;38:2007–24.
[25] Klug JH. High-performance adhesive systems for polymer composite bonding applications. PhD thesis, University of Washington; 1999.
[26] Liotier PJ. Microcracking of composites reinforced by multiaxial multiply stitched preforms under cyclical hygrothermal loading. PhD Thesis. Ecole des Mines de Saint-Etienne; 2008.
[27] Gigliotti M, Jacquemin F, Vautrin A. On the maximum curvatures of 0/90 plates under thermal stress. Compos Struct 2005;68(2):77–184.
[28] Liotier PJ, Vautrin A, Beraud JM, Henrat P. Introduction to the characterization of hygrothermal microcracking of crossply composites reinforced by stitched non-woven UD laminae. Appl Mech Sand Mater 2008;13–14:77–83.
[29] Mattsson D, Joffe R, Varna J. Damage in NCF composites under tension: effect of layer stacking sequence. Eng Fract Mech 2008;75(9):2666–82.
[30] Mikhaluk DS, Truong TC, Borovkov AI, Lomov SV, Verpoest I. Experimental observations and finite element modelling of damage initiation and evolution in carbon/epoxy non-crimp fabric composites. Eng Fract Mech 2008;75(9):2751–66.